IOP PUBLISHING NANOTECHNOLOGY

Nanotechnology **19** (2008) 445717 (9pp) doi:10.1088/0957-4484/19/44/445717

# High-resolution and large dynamic range nanomechanical mapping in tapping-mode atomic force microscopy

**Ozgur Sahin**[1,3] **and Natalia Erina**[2]

[1] The Rowland Institute at Harvard, Harvard University, Cambridge, MA 02142, USA
[2] Veeco Instruments, Santa Barbara, CA 93117, USA

E-mail: sahin@rowland.harvard.edu

Received 5 August 2008, in final form 4 September 2008
Published 2 October 2008
Online at stacks.iop.org/Nano/19/445717

**Abstract**

High spatial resolution imaging of material properties is an important task for the continued development of nanomaterials and studies of biological systems. Time-varying interaction forces between the vibrating tip and the sample in a tapping-mode atomic force microscope contain detailed information about the elastic, adhesive, and dissipative response of the sample. We report real-time measurement and analysis of the time-varying tip–sample interaction forces with recently introduced torsional harmonic cantilevers. With these measurements, high-resolution maps of elastic modulus, adhesion force, energy dissipation, and topography are generated simultaneously in a single scan. With peak tapping forces as low as 0.6 nN, we demonstrate measurements on blended polymers and self-assembled molecular architectures with feature sizes at 1, 10, and 500 nm. We also observed an elastic modulus measurement range of four orders of magnitude (1 MPa to 10 GPa) for a single cantilever under identical feedback conditions, which can be particularly useful for analyzing heterogeneous samples with largely different material components.

(Some figures in this article are in colour only in the electronic version)

M This article features online multimedia enhancements

## 1. Introduction

Engineered nanomaterials and biological samples often exhibit heterogeneity in material characteristics and chemical composition. Imaging these samples with nanoscale resolution to identify surface topography and composition is of great importance for the development of advanced materials and understanding biological systems. Tapping-mode atomic force microscopy (TM-AFM) is a widely used nanoscale imaging technique for topographical and compositional mapping due to the gentle forces involved, minimal lateral interaction, and high spatial resolution [1, 2]. This operation mode relies on a cantilever vibrating on resonance near the surface. The tip of the cantilever intermittently strikes the surface with sufficiently large amplitudes to eliminate sticking of the tip to the surface. Due to vibrations, tip–sample interaction forces are time dependent and they contain information on the elastic, viscoelastic, and adhesive properties of the sample.

In tapping mode, material composition mapping is performed by recording the phase of the cantilever vibrations [3]. The phase signal is a measure of the energy dissipation during the tip–sample interactions [4], which is determined by the interplay between the viscoelastic and adhesive properties of the sample. Therefore, it has been difficult to relate phase images to a specific material property. In order to measure elastic, viscous, and adhesive properties of samples, researchers use different atomic force microscopy techniques such as force volume [5], pulsed force mode [6], force modulation microscopy [7], and ultrasonic and acoustic AFM [8–10]. In particular, contact resonance based techniques have demonstrated quantitative and accurate elastic modulus mapping [11, 12].

The dynamics of the tapping cantilever have been studied widely to extract more detailed information about the sample

[3] Author to whom any correspondence should be addressed.

 

material properties [13]. Relationships between the steady state vibration amplitude, phase, and tip–sample forces have been established [14–17]. These investigations showed that except for the overall tip–sample energy dissipation, much of the information about sample properties is lost or convoluted. Nevertheless, force spectroscopic methods have demonstrated the recovery of tip–sample interaction potentials [18, 19] and identification of energy dissipation processes [20].

Realization of the information loss in phase images was followed by investigations of higher-harmonic vibrations of the cantilever [21, 22]. These high frequency vibrations are excited due to the nonlinear spatial dependency of the tip–sample interaction, which translates into time-varying forces as the tip is moving back and forth against the sample. Thus, higher harmonics have the potential to recover the information about tip–sample interactions. Imaging and reconstruction of time-varying forces with higher harmonics have been demonstrated in both ambient [23–25] and liquids [26, 27]. Despite the vast potential of higher harmonics, the low signal to noise ratio of the high frequency vibrations and difficulties in calibrating the cantilever frequency response have limited their widespread use.

Recently, various groups have made attempts to improve efficient access to high frequency components of the tip–sample forces. Simultaneous excitation and detection of multiple eigenmodes of the cantilever [28–31], improving the response of the cantilever at high frequencies through geometric design [32], adaptation of sensitive and ultra-wide bandwidth ultrasonic transducers as force sensors [33, 34], and integrating a diffraction grating into the cantilever [35] can be listed among these approaches.

Recently introduced T-shaped AFM cantilevers have enabled the measurement of time-varying tip–sample forces with good signal to noise ratio [36, 37]. These cantilevers are called torsional harmonic cantilevers (THC) and they have their tips at an offset distance from the longitudinal axis (figure 1), which allows using faster torsional modes to measure the time-varying tip–sample force waveforms during the vertical oscillations of the tip. High-speed force–distance curves can be generated from the time-varying forces to extract material properties of the sample.

In this paper, we report real-time measurement of time-varying tip–sample forces and mapping of material properties like elasticity and adhesion with high spatial resolution and gentle forces in TM-AFM through the use of the THC. We have implemented the mathematical procedures and physical models described in [36] in a computer program to measure tip–sample force waveforms and calculate the local elastic modulus (see experimental details section for a brief description). The speed of the calculations permits real-time detailed mechanical analysis as the surface is scanned in TM-AFM. We also improved the THC design by placing the tip further away from the longitudinal axis and applying reflective aluminum coating on the backside of the cantilever. The former modification improved the sensitivity and the latter reduced the noise in the lateral detector signal, as well as false higher-harmonic contributions due to substrate reflections. These improvements enable real-time mapping of local elastic response with peak tapping forces as low as 600 pN and indentation depths in the angstrom scale, suitable for high spatial resolution mapping of material properties. A supplementary movie file (available at stacks.iop.org/Nano/19/445717) based on experimental data illustrates the real-time visualization capability of time-varying tip–sample force measurements and mapping of elastic modulus across the surface of a multilayer polyethylene sample composed of high density and low density regions.

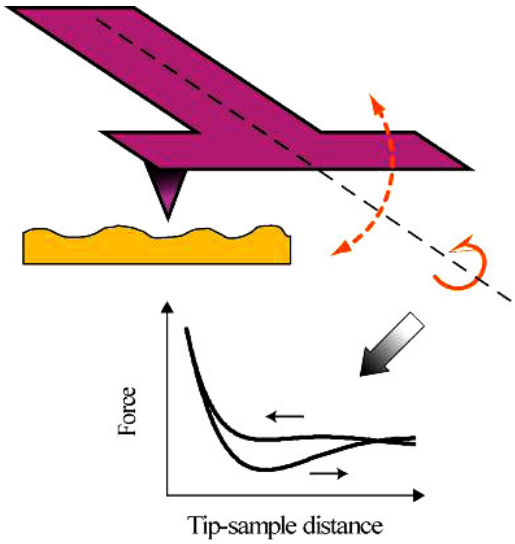


**Figure 1.** Schematic diagram of the torsional harmonic cantilever operation. The T-shaped cantilever with an offset tip is vibrated vertically at its resonance frequency. Tip–sample interactions twist the cantilever and generate torsional vibrations. Detected torsional motion is used to generate high-speed force–distance curves.

## 2. Experimental details

### *2.1. Experimental setup*

A commercial AFM system (Multimode™ series with a Nanoscope 5 controller, and a signal breakout box) has been used. Cantilever vibration signals are collected with a data acquisition card (NI-DAQ S-series 6115). Calculation of elastic modulus values from the torsional vibration signals is performed with a personal computer equipped with two processors (3.2 GHz, 2 GB shared memory).

### *2.2. Torsional harmonic cantilevers*

THCs were fabricated using the conventional manufacturing processes of commercial probes (single crystal silicon), but with a custom T-shaped geometry and offset tip. The backsides of the THCs are coated with aluminum to reduce reflections from the substrate. Two different THC designs were used in this study. The first THC is used in the experiments for figures 2 and 3. It is 300 $\mu$m long, 30 $\mu$m wide, and approximately 4.5 $\mu$m thick. The tip offset distance is 22 $\mu$m. The free end of the cantilever is 55 $\mu$m wide. The torsional resonance frequency of this cantilever is 905.3 KHz. The ratio of torsional to vertical resonance frequencies is 16.35. The second THC is used in the experiments for figure 4. It is

180 $\mu$m long, 20 $\mu$m wide, and approximately 3 $\mu$m thick. The tip offset distance is 20 $\mu$m. The free end of the cantilever is 50 $\mu$m wide. The torsional resonance frequency of this cantilever is 837.2 kHz. The ratio of the torsional to the vertical resonance frequency is 9.44.

### *2.3. Tapping-mode feedback conditions*

Spring constant $K$, drive $\omega_{dr}$ and resonance $\omega_0$ frequencies, set point $A_s$ and free amplitudes $A_0$ for the experiments were as follows: figure 2: $K = 2.6$ N m$^{-1}$, $\omega_{dr} = 55.0$ kHz, $\omega_0 = 55.36$ kHz, $A_s = 31$ nm, $A_0 = 38$ nm. Figure 3: $K = 2.6$ N m$^{-1}$ $\omega_{dr} = \omega_0 = 55.37$ kHz, $A_s = 49$ nm, $A_0 = 64$ nm. Figure 4: $K = 2.4$ N m$^{-1}$ $\omega_{dr} = \omega_0 = 88.64$ kHz, $A_s = 13$ nm, $A_0 = 15$ nm.

### *2.4. Calibration and calculation of tip–sample forces*

We used the previously described mathematical procedures to reconstruct the tip–sample force waveform from the raw deflection signals [36]. The elements of this procedure are: averaging vibration waveforms over several consecutive oscillation cycles to reduce noise, correcting the effect of the torsional frequency response, and eliminating the cross-talk from large vertical signals. The calculations are carried out in the form of matrix multiplication in Labview. Elements of this matrix are calculated once at the beginning of the imaging process. We followed the same procedure for cross-talk elimination as in [36] where a linear curve fitting procedure is used. After these linear steps, the waveform still remains in voltage units. Calibration of this signal (i.e. volts to Newtons conversion) is performed according to [38]. That procedure requires peak tip–sample forces of around 10 nN. For the ultra-sharp tip, we used calibration parameters of another cantilever from the same batch with a similar resonance frequency. The number of cycles to average is chosen to obtain a data rate of 1 kHz for the experiments in figures 2 and 4, and 1.5 kHz for figure 3.

### *2.5. Contact mechanics model and curve fitting*

We used the Derjaguin–Muller–Toporov (DMT) model to estimate the elastic modulus [39]. According to this model the forces during the indentation are described by the following equation:

$$F_{\text{interaction}} = \tfrac{4}{3} E^* \sqrt{R} (d - d_0)^{3/2} + F_{\text{adh}}. \qquad (1)$$

Here $F_{\text{interaction}}$ is the tip–sample force, $E^*$ is the reduced elastic modulus of the tip and the sample, $R$ is the tip radius, $d_0$ is the surface rest position, $d - d_0$ is the depth of indentation, and $F_{\text{adh}}$ is the constant adhesion force during the contact. A more detailed model is the JKR model, which provides better results on compliant samples (1–10 MPa). However, lack of an explicit relationship between force and indentation makes it difficult to compute the modulus within the limited time budget. Furthermore, materials exhibit a viscoelastic response and the adhesion forces depend on the indentation depth. In addition, better approximations for the tip geometry can be obtained by electron microscopy and incorporated in the calculations [40]. Due to the limited time budget on each pixel of an image, the calculations have to be fast. The DMT model provides a reasonable compromise between the details and simplicity in calculations in this initial demonstration.

We estimate the reduced elastic modulus of the sample by fitting equation (1) to the tip–sample forces. Curve fitting is performed by first approximating the term $F_{\text{adh}}$ with the peak negative force during the retraction of the tip. Then, forces ($F_{\text{interaction}} - F_{\text{adh}}$) at the points between peak repulsive and peak attractive forces (unloading portion of the curve) are raised to the power 2/3 and linearly fitted to calculate the scalar multiplier. The linear fit did not use data points where forces were less than 20% of the peak indentation force. The reduced elastic modulus can be obtained from the scalar multiplier with the knowledge of the tip radius. We used 7 nm tip radius for the measurements in figures 2 and 3 (characterized by blind reconstruction from the image of a sample with sharp edges), and 1 nm for the measurements in figure 4.

### *2.6. Materials and sample preparation*

The following materials have been used in this study.

(I) Homogeneous materials. (Here by 'homogeneous' we consider one-component materials, amorphous or semicrystalline, organic or inorganic.) The materials used in figure 2 with their nominal elastic modulus values are as follows: polydimethylsiloxanes (PDMS) with different ratios of the polymer and the hardener 1:10 (1 MPa) and 1:15 (0.5 MPa) (Sigma); low density polyethylenes (LDPE) with different densities: LDPE_1 (0.87 g cm$^{-3}$, 50 MPa) and LDPE_2 (0.94 g cm$^{-3}$, 300 MPa); high density polyethylene HDPE (0.75 GPa); polypropylene PP (1.2 GPa); polystyrene PS (4 GPa), (all from Polymer Sources, Inc.); highly oriented pyrolytic graphite GRP (5 GPa); mica (50 GPa). All polymer samples for AFM experiments were prepared in the form of sheets by hot-press melting and subsequent cooling.

(II) Heterogeneous materials. A—thermoplastic vulcanizate (TPV) based on polypropylene (PP) and ethylene-propylene-diene monomer elastomer (EPDM). To access the bulk morphology, TPV was cryomicrotomed at −100 °C using a diamond knife ('MicroStar Tech, TS). B—commercially available triblock-copolymer of polymethylmethacrylate-polyisobutylene-polymethylmethacrylate (PMMA-PIB-PMMA) was spin-cast from xylene solution on a piece of silicon wafer. The film thickness is ∼1 $\mu$m.

(III) Self-assembled alkanes. The xylene solution of a commercially available short-chain alkane $C_{32}H_{74}$ (Polymer Sources, Inc) was spin-cast on graphite.

## 3. Results and discussion

Real-time analysis of tip–sample force waveforms allows us to measure and map reduced elastic modulus and adhesion force of the sample during the imaging process. We

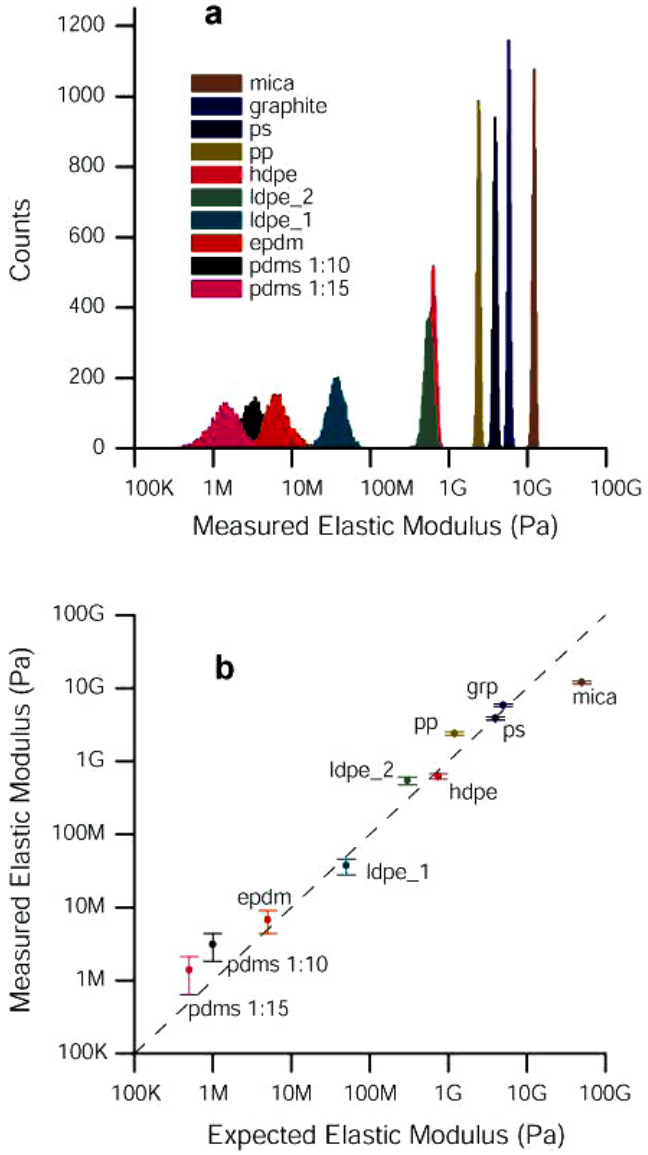


**Figure 2.** Large dynamic range nanomechanical measurements. (a) Histograms of calculated elastic modulus values on different samples. Histograms are generated by 5000 consecutive measurements, 1 ms per data point. (b) Mean values of the histograms are plotted against nominal elastic modulus values of the samples. Standard deviations derived from the histograms are shown as error bars.

have performed experiments on a variety of samples to observe the accuracy, range, and spatial resolution of these nanomechanical measurements.

### *3.1. Elastic modulus measurements with large dynamic range*

We first investigate the range of elastic modulus values that can be measured by the same THC under identical feedback conditions (i.e. imaging conditions). This analysis will help determine the minimum detectible elastic modulus level and the point where the measured values are saturating. It will also serve as a test to compare the measured values with the expected ones.

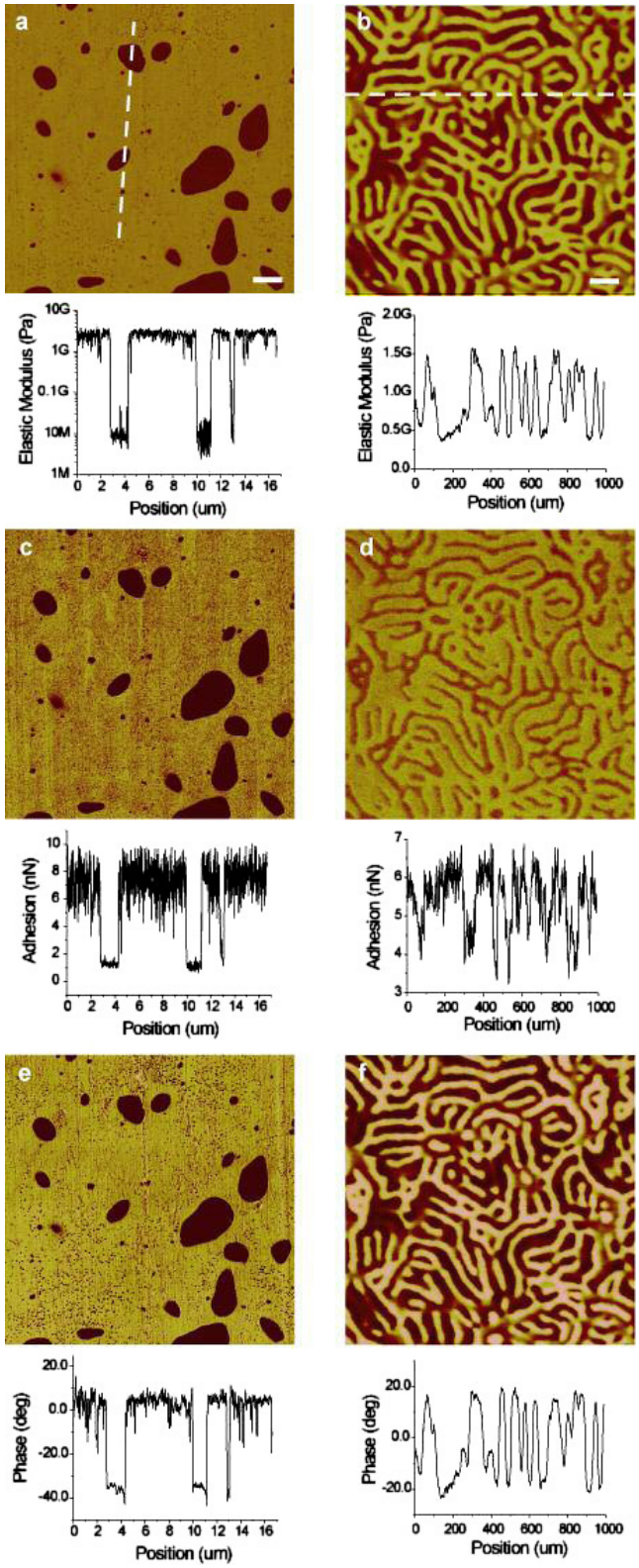


**Figure 3.** Nanomechanical mapping in the tapping mode. Thermoplastic vulcanizate (left column) and PMMA-PIB-PMMA block-copolymer film (right column) are scanned in tapping mode. High-speed force–distance curves are used to estimate local elastic modulus ((a), (b)) and peak adhesion force ((c), (d)). Conventional phase images are given in ((e), (f)). All three images are generated simultaneously. Numeric values in each image across the sections indicated by the dashed lines in ((a), (b)) are given below the images. Scale bars are (a) 2 $\mu$m, (b) 100 nm. Colored images in (a) and (b) are generated according to logarithms of elastic moduli.

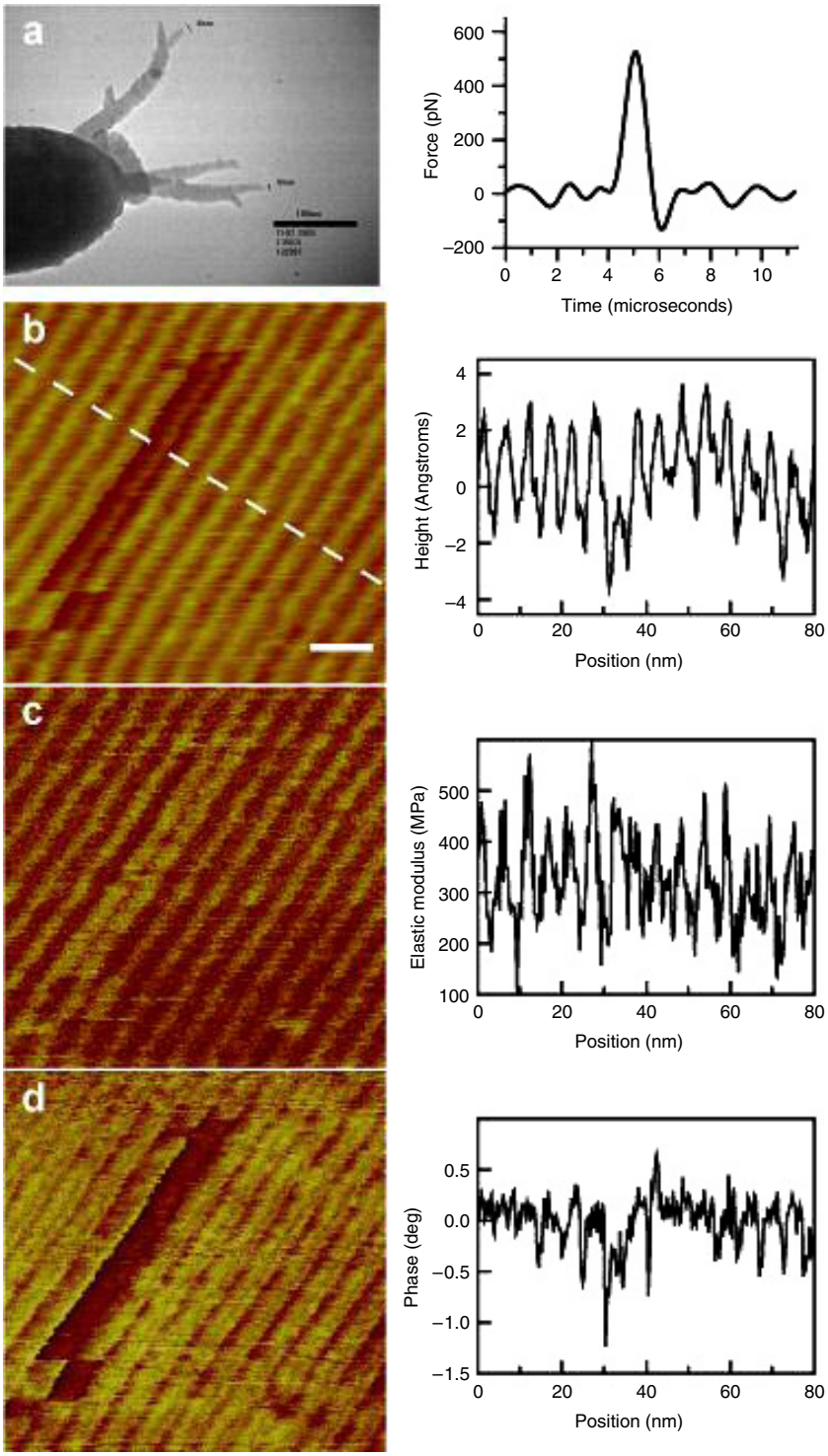


**Figure 4.** High-resolution mechanical mapping across the molecular self-assembly of $C_{32}H_{74}$ alkane layers on graphite. (a) TEM picture of the carbon spikes grown on the THC and an example of the tip–sample force waveform recorded with this tip during the experiments (right). Scale bar in (a), 100 nm. Simultaneously recorded topography (b), elastic modulus (c), and phase images (d) are given with section plots on the right. Scale bar in (b) 10 nm.

Figure 2(a) shows histograms of elastic modulus measurements on a variety of macroscopically homogeneous samples under identical tapping-mode feedback conditions. Each data point on these histograms is calculated based on the tip–sample force waveforms averaged over consecutive cycles within 1 ms. The curves are analyzed according to the numerical procedures described in section 2.5 to calculate the corresponding reduced elastic modulus values. We observe that the standard deviations of the measurements increase towards more compliant samples. This is due to the reduction in peak tapping forces on compliant samples [41], which hinders estimation of the elastic modulus due to noise. Namely,

at around 1 MPa of sample stiffness, tip–sample forces reduce to the noise level, and the standard deviation in elastic modulus measurements reaches up to 50% of the nominal value. So, this sets a lower limit in our elastic modulus measurements. Mean values and standard deviations of the histograms are compared to the nominal bulk values of each sample in figure 2(b). Perfect agreement between the calculated and the nominal bulk values is not expected, since the elastic moduli of these samples depend on the thermal history, cross-linking density of the rubbers, frequency of the measurements, and differences between surface and bulk properties of the sample. Furthermore, our contact mechanics model does not incorporate viscosity of the samples. Nevertheless, there is a fair degree of consistency between the measurements and typical bulk values, though with two critical deviations.

We have found that the calculated moduli of the two grades of PDMS samples with different cross-link density are overestimated. This is most likely a consequence of the frequency dependent mechanical behavior of rubbery materials [42]. These measurements are performed at 55 kHz, well above the conventional frequency range (1–100 Hz). Measurements on rubbery materials near their glass transition temperatures are affected the most by high frequency measurements. It is worth emphasizing that measurements on such materials should be interpreted carefully. In general, any scanning type measurement would be subject to frequency dependent behavior of the materials, because the time spent on each pixel is about a millisecond or less at typical scan rates.

The second prominent deviation between the measured and expected values is observed on mica, where the elastic modulus is significantly underestimated (12 GPa versus 50 GPa). Theoretical studies of the tapping mode have shown that tip–sample contact durations shorten towards stiffer samples [43]. Beyond a certain level of sample stiffness, torsional vibrations cannot follow time-varying tip–sample forces closely. This would result in a wider force waveform being measured, which will be similar to the waveform of a more compliant sample. Thus, the finite bandwidth of torsional vibrations introduces a saturation mechanism to the measurements by the THC.

In the above analysis, anisotropic elastic properties of the tip and the sample, finite reduced modulus of the silicon tip, and the effect of Poisson's ratio in reduced elastic modulus calculations are not taken into account. These effects can lead to deviations from the actual elastic modulus values. For materials with anisotropic elastic response, appropriate mechanical models should be used. Nevertheless, the results in figure 2 demonstrate that under typical tapping-mode operating conditions reduced elastic modulus measurements can be performed over four orders of magnitude; from 1 MPa to 10 GPa. This range is sufficient to perform mechanical property mapping over a wide spectrum of heterogeneous materials. In addition, by using tips with larger apex diameter and cantilevers with lower vertical spring constants, it should also be possible to perform measurements of even more compliant materials.

### *3.2. High-resolution mapping of elasticity and adhesion forces in tapping-mode AFM*

Here we investigate the ability to conduct high spatial resolution mechanical measurements. Figure 3 demonstrates simultaneously generated maps of reduced elastic modulus ((a), (b)), peak attractive force, or adhesion ((c), (d)), and conventional phase ((e), (f)) for two heterogeneous samples; TPV and a triblock-copolymer PMMA-PIB-PMMA with a lamellar phase-separated morphology. These kinds of samples are widely studied by AFM techniques [44, 45]. Both samples consist of stiff and compliant components, yet the morphological organization in terms of feature dimensions and spacing between them are substantially different. We will start with the discussion of the reduced elastic modulus maps. TPV is widely used in the modern automotive industry due to its unique combination of mechanical and rheological properties: high flexibility and elongation but low residual set and easy processing, unusual for traditional rubbers. As can be seen in figure 3(a), the more compliant EPDM is confined to micron sized domains in the stiff PP matrix. Modulus values across a section of the image reveal more than two orders of magnitude difference between PP (∼2 GPa) and EPDM (5–10 MPa) regions. These values are close to the corresponding bulk sample values in figure 2. Contrary to the observations in TPV, the block-copolymer exhibits mechanical properties that are different from the corresponding bulk values. Figure 3(b) shows the mechanical map of the block-copolymer. The corresponding modulus profile across a section reveals the two chemical blocks with a variation of modulus values, from 0.5 to 1.5 GPa. We also see that modulus values transition from low to high values at distances around of 10 nm.

PIB is a rubbery material with elastic modulus ∼5 MPa; therefore, the observed elastic modulus on PIB blocks (0.5 GPa) demonstrates a dramatic increase in stiffness. While high frequency of measurements can account for an increase in stiffness, geometrical confinement can be another mechanism that results in increased stiffness. Mechanical properties of materials strongly depend on their micro and nanoscale structure. Geometric confinement enhances molecular and supramolecular ordering, and emphasizes the roles of surface tension and surface stress. Therefore, confinement can alter mechanical properties dramatically. For example, substantial increments in elastic modulus have been reported in tensile measurements of polymer nanotubes [46], nanofibers [47], and in AFM based measurements of zinc oxide nanowires [48] with diameters less than 100 nm. The block-copolymer sample investigated here exhibits domains that are approximately 50 nm wide and therefore its elastic properties could be influenced by confinement effects.

We have also recorded the peak attractive forces as a measure of adhesive properties for both polymer samples in figure 3. The resulting images and respective cross section data are given in figures 3(c) and (d). In the case of the TPV sample, we see that peak attractive forces are less on the rubbery regions. There is also a significant variation in attractive forces on the stiff PP regions. A closer look at the image data shows that this variation is not due to noise. There is a substantial local variation of the measured values,

which may be due to the surface roughness introduced in the cutting process of the sample. On the second sample, the peak attractive force map differentiates the two chemical blocks of the copolymer. However, the force contrast between the two regions is inverted in comparison to the elasticity map; the stiffer PMMA regions provide less attractive force than the compliant PIB regions. Noise also becomes more visible because the difference in peak attractive forces for the two regions is about 2 nN and it is approaching the force noise (∼0.25 nN, rms). It is important to note that adhesion forces caused by the formation and disruption of capillary necks can happen much more rapidly than the response speed of the torsional mode. The two images presented show a distinct contrast mechanism based on attractive forces. However, we believe further experimental and theoretical work is necessary to assess the reliability of adhesion force measurements and relate them to specific surface energies.

Figures 3(e) and (f) show simultaneously recorded conventional phase images of the TPV and block-copolymer samples. As we mentioned before, phase contrast is primarily determined by the energy dissipation during tip–sample interactions. Capillary forces and adhesion hysteresis are two contributors to the energy dissipation, which are mediated by attractive forces. However, their influence depends on the tip–sample contact area which further depends on the compliance of the sample. The viscous response of the sample can also contribute to energy dissipation due to finite speed of the tip while in contact with the sample. In general, lower stiffness and larger attractive forces increase the energy dissipation. The two samples investigated in figure 3 exhibit both stiffness and adhesion force contrast. However, the contrasts in both phase images appear to be correlated to the corresponding reduced elastic modulus maps. Despite their largely different elastic modulus values and morphological organization, phase values plotted across sections of each image show that phase contrast is approximately the same (∼40°) for both samples. This is most likely due to the joint contributions of adhesive and viscoelastic properties into overall energy dissipation. Note that the compliant regions of the TPV sample are the less adhesive regions as well. However, the compliant regions of the block-copolymer sample are the more adhesive regions of that sample.

For the samples discussed above, the mechanical properties are primarily determined by the supramolecular organization within each chemical component. Mechanical properties can also vary across molecular length scales and contain information about the strength and organization of chemical bonds and physical interactions. To demonstrate this potential we have studied the surface formed by self-assembling ultra-thin layers of $C_{36}H_{74}$ alkane chains on graphite. Such systems have been studied extensively by scanning tunneling microscopy (STM) and AFM [49, 50] techniques because of their potential as novel platforms for molecular electronics, energy harvesting, and also to understand molecular self-assembly phenomena at a fundamental level.

To obtain sub-molecular spatial resolution, carbon spike tips [2] with apex radius around 1 nm have been grown on THC. Peak tapping forces were kept at extremely low levels ∼0.6 nN to minimize contact pressure (see figure 4(a)). The topography image and section data in figure 4(b) show the periodical structure of closed packed lamellar ribbons of ∼4.7 nm in width, matching the molecular length of $C_{36}H_{74}$ in fully extended conformation. STM studies showed that the carbon backbone consisting of $–CH_2-$ groups are aligned parallel to the substrate and perpendicular to the ribbon edges [49]. A simultaneously recorded reduced elastic modulus map (figure 4(c)) and the modulus profile across a section reveal that topographically higher regions are about a factor of two stiffer than the lower regions. The widths of the stiff regions are approximately 1.5 nm. We believe the compliant regions reflect the $–CH_3$ end group position. The end groups are more flexible and hence less stiff because they are covalently connected to the backbone only from one side. However, modeling of contact mechanics and even quantities like stress, strain, and contact area are not clearly defined at the sub-molecular scale and they can be influenced by angstrom scale corrugations of the molecules. Therefore, molecular scale measurements can be best interpreted in the light of numerical simulations. A simultaneously recorded phase image in figure 4(d) also shows the periodical structure of the lamellar ribbons. However, phase contrast is found to be very small (∼0.5°), presumably due to reduced attractive forces on the ultra-sharp tip. Reduced forces also resulted in a lack of contrast in the peak attractive force map due to force noise (data not shown).

## 4. Conclusions

To summarize, we have investigated nanomechanical mapping by the real-time analysis of time-varying tip–sample forces in tapping-mode AFM. For the first time in tapping mode we have generated maps of local elastic modulus and adhesion forces together with conventional phase and topography images. The resulting nanomechanical maps showed a typical spatial resolution of 10 nm. With the use of ultra-sharp carbon tips and peak forces less than 1 nN the resolution reached 1.5 nm. Most importantly, we observed a large dynamic range in elastic modulus measurements, which will be particularly useful in the analysis of heterogeneous samples with large and small variations in material properties. These results suggest that tapping-mode AFM, combined with specially designed cantilevers, has the potential to perform detailed nanomechanical analysis of samples with gentle forces and high spatial resolution. While the current state of the presented technique allows investigations of mechanical properties of a wide range of materials, further technical improvements can enable measurement of electrical and magnetic forces, as well as measurements in liquids to study mechanical properties of biomolecules and cells at high spatial resolution.

## Acknowledgments

This work was supported by the Rowland Junior Fellows program. The authors thank Sergei Magonov for valuable discussions and comments. The cantilevers used in this study were kindly provided by Veeco Probes and MikroMasch.

## References


[1] Zhong Q, Inniss D, Kjoller K and Elings V B 1993 Fractured polymer silica fiber surface studied by tapping mode atomic-force microscopy *Surf. Sci.* **290** L688–92

[2] Klinov D and Magonov S 2004 True molecular resolution in tapping-mode atomic force microscopy with high-resolution probes *Appl. Phys. Lett.* **84** 2697–9

[3] Garcia R, Magerle R and Perez R 2007 Nanoscale compositional mapping with gentle forces *Nat. Mater.* **6** 405–11

[4] Cleveland J P, Anczykowski B, Schmid A E and Elings V B 1998 Energy dissipation in tapping-mode atomic force microscopy *Appl. Phys. Lett.* **72** 2613–5

[5] Butt H J, Cappella B and Kappl M 2005 Force measurements with the atomic force microscope: technique, interpretation and applications *Surf. Sci. Rep.* **59** 1–152

[6] RosaZeiser A, Weilandt E, Hild S and Marti O 1997 The simultaneous measurement of elastic, electrostatic and adhesive properties by scanning force microscopy: pulsed-force mode operation *Meas. Sci. Technol.* **8** 1333–8

[7] Radmacher M, Tilmann R W and Gaub H E 1993 Imaging viscoelasticity by force modulation with the atomic force microscope *Biophys. J.* **64** 735–42

[8] Yamanaka K, Noguchi A, Tsuji T, Koike T and Goto T 1999 Quantitative material characterization by ultrasonic AFM *Surf. Interface Anal.* **27** 600–6

[9] Rabe U, Amelio S, Kester E, Scherer V, Hirsekorn S and Arnold W 2000 Quantitative determination of contact stiffness using atomic force acoustic microscopy *Ultrasonics* **38** 430–7

[10] Huey B D 2007 AFM and acoustics: fast, quantitative nanomechanical mapping *Ann. Rev. Mater. Res.* **37** 351–85

[11] Stan G and Cook R F 2008 Mapping the elastic properties of granular Au films by contact resonance atomic force microscopy *Nanotechnology* **19** 235701

[12] Stan G and Price W 2006 Quantitative measurements of indentation moduli by atomic force acoustic microscopy using a dual reference method *Rev. Sci. Instrum.* **77** 103707

[13] Raman A, Melcher J and Tung R 2008 Cantilever dynamics in atomic force microscopy *Nano Today* **3** 20–7

[14] Tamayo J and Garcia R 1998 Relationship between phase shift and energy dissipation in tapping-mode scanning force microscopy *Appl. Phys. Lett.* **73** 2926–8

[15] San Paulo A and Garcia R 2001 Tip–surface forces, amplitude, and energy dissipation in amplitude-modulation (tapping mode) force microscopy *Phys. Rev.* B **64** 193411

[16] Lee S I, Howell S W, Raman A and Reifenberger R 2002 Nonlinear dynamics of microcantilevers in tapping mode atomic force microscopy: a comparison between theory and experiment *Phys. Rev.* B **66** 115409

[17] Durig U 2000 Interaction sensing in dynamic force microscopy *New J. Phys.* **2** 1–12

[18] Holscher H 2006 Quantitative measurement of tip–sample interactions in amplitude modulation atomic force microscopy *Appl. Phys. Lett.* **89** 123109

[19] Hu S and Raman A 2008 Inverting amplitude and phase to reconstruct tip–sample interaction forces in tapping mode atomic force microscopy *Nanotechnology* **19** 375704

[20] Garcia R, Gomez C J, Martinez N F, Patil S, Dietz C and Magerle R 2006 Identification of nanoscale dissipation processes by dynamic atomic force microscopy *Phys. Rev. Lett.* **97** 016103

[21] Hillenbrand R, Stark M and Guckenberger R 2000 Higher-harmonics generation in tapping-mode atomic-force microscopy: Insights into the tip–sample interaction *Appl. Phys. Lett.* **76** 3478–80

[22] Stark R W and Heckl W M 2000 Fourier transformed atomic force microscopy: tapping mode atomic force microscopy beyond the Hookian approximation *Surf. Sci.* **457** 219–28

[23] Crittenden S, Raman A and Reifenberger R 2005 Probing attractive forces at the nanoscale using higher-harmonic dynamic force microscopy *Phys. Rev.* B **72** 235422

[24] Stark M, Stark R W, Heckl W M and Guckenberger R 2002 Inverting dynamic force microscopy: from signals to time-resolved interaction forces *Proc. Natl Acad. Sci. USA* **99** 8473–8

[25] Stark R W and Heckl W M 2003 Higher harmonics imaging in tapping-mode atomic-force microscopy *Rev. Sci. Instrum.* **74** 5111–4

[26] Legleiter J, Park M, Cusick B and Kowalewski T 2006 Scanning probe acceleration microscopy (SPAM) in fluids: mapping mechanical properties of surfaces at the nanoscale *Proc. Natl Acad. Sci. USA* **103** 4813–8

[27] Preiner J, Tang J L, Pastushenko V and Hinterdorfer P 2007 Higher harmonic atomic force microscopy: imaging of biological membranes in liquid *Phys. Rev. Lett.* **99** 046102

[28] Martinez N F, Patil S, Lozano J R and Garcia R 2006 Enhanced compositional sensitivity in atomic force microscopy by the excitation of the first two flexural modes *Appl. Phys. Lett.* **89** 153115

[29] Proksch R 2006 Multifrequency, repulsive-mode amplitude-modulated atomic force microscopy *Appl. Phys. Lett.* **89** 113121

[30] Stark R W, Naujoks N and Stemmer A 2007 Multifrequency electrostatic force microscopy in the repulsive regime *Nanotechnology* **18** 065502

[31] Bostanci U, Abak M K, Aktas O and Dana A 2008 Nanoscale charging hysteresis measurement by multifrequency electrostatic force spectroscopy *Appl. Phys. Lett.* **92** 093108

[32] Sadewasser S, Villanueva G and Plaza J A 2006 Special cantilever geometry for the access of higher oscillation modes in atomic force microscopy *Appl. Phys. Lett.* **89** 033106

[33] Balantekin M, Onaran A G and Degertekin F L 2008 Quantitative mechanical characterization of materials at the nanoscale through direct measurement of time-resolved tip–sample interaction forces *Nanotechnology* **19** 085704

[34] Onaran A G, Balantekin M, Lee W, Hughes W L, Buchine B A, Guldiken R O, Parlak Z, Quate C F and Degertekin F L 2006 A new atomic force microscope probe with force sensing integrated readout and active tip *Rev. Sci. Instrum.* **77** 023501

[35] Sarioglu A F and Solgaard O 2008 Cantilevers with integrated sensor for time-resolved force measurement in tapping-mode atomic force microscopy *Appl. Phys. Lett.* **93** 023114

[36] Sahin O, Magonov S, Su C, Quate C F and Solgaard O 2007 An atomic force microscope tip designed to measure time-varying nanomechanical forces *Nat. Nanotechnol.* **2** 507–14

[37] Sahin O 2008 Time-varying tip–sample force measurements and steady-state dynamics in tapping-mode atomic force microscopy *Phys. Rev.* B **77** 115405

[38] Sahin O 2007 Harnessing bifurcations in tapping-mode atomic force microscopy to calibrate time-varying tip–sample force measurements *Rev. Sci. Instrum.* **78** 103707

[39] Israelachvili J 2003 *Intermolecular and Surface Forces* (London: Academic)

[40] Sergey B *et al* 2007 Theoretical modelling and implementation of elastic modulus measurement at the nanoscale using atomic force microscope *J. Phys.: Conf. Ser.* **61** 1303

[41] Hu S Q and Raman A 2007 Analytical formulas and scaling laws for peak interaction forces in dynamic atomic force microscopy *Appl. Phys. Lett.* **91** 123106

[42] Ward I M 2004 *An Introduction to the Mechanical Properties of Solid Polymers* (Chichester: Wiley)

[43] Tamayo J and Garcia R 1996 Deformation, contact time, and phase contrast in tapping mode scanning force microscopy *Langmuir* **12** 4430–5

[44] Magonov S N and Reneker D H 1997 Characterization of polymer surfaces with atomic force microscopy *Annu. Rev. Mater. Sci.* **27** 175–222

[45] Tsukruk V V 1997 Scanning probe microscopy of polymer surfaces *Rubber Chem. Technol.* **70** 430–67
[46] Cuenot S, Demoustier-Champagne S and Nysten B 2000 Elastic modulus of polypyrrole nanotubes *Phys. Rev. Lett.* **85** 1690–3
[47] Arinstein A, Burman M, Gendelman O and Zussman E 2007 Effect of supramolecular structure on polymer nanofibre elasticity *Nat. Nanotechnol.* **2** 59–62
[48] Stan G, Ciobanu C V, Parthangal P M and Cook R F 2007 Diameter-dependent radial and tangential elastic moduli of ZnO nanowires *Nano Lett.* **7** 3691–7
[49] De Feyter S and De Schryver F C 2003 Two-dimensional supramolecular self-assembly probed by scanning tunneling microscopy *Chem. Soc. Rev.* **32** 139–50
[50] Magonov S N and Yerina N A 2003 High-temperature atomic force microscopy of normal alkane C60H122 films on graphite *Langmuir* **19** 500–4